NMR Crystallography

DOI: 10.1002/anie.200805302

Crystal-Structure Determination of Powdered Paramagnetic Lanthanide Complexes by Proton NMR Spectroscopy**

*Gwendal Kervern, Anthony D'Aléo, Loïc Toupet, Olivier Maury, Lyndon Emsley, and Guido Pintacuda**

Solid-state NMR spectroscopy is emerging as a powerful tool to address the characterization of challenging materials.[1] For molecular solids at natural isotopic abundance, this advance has now reached the stage at which crystal structures of powdered samples can be successfully validated or determined by solid-state NMR spectroscopy.[2] However, these methods cannot be directly applied to paramagnetic compounds, since nuclear spin dynamics are profoundly affected by unpaired electrons.

Herein, we propose a protocol for structure determination of powdered microcrystalline paramagnetic solids at natural isotopic abundance. The protocol makes use of paramagnetic effects to simultaneously define the conformation of a molecule in the lattice and the intermolecular packing in the solid phase. Our purpose is illustrated on a family of lanthanide compounds **1**–**3**.[3]

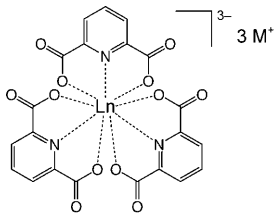

1a: Ln=Yb, M=Cs
1b: Ln=Yb, M=Na
2a: Ln=Tb, M=Cs
2b: Ln=Tb, M=Na
3a: Ln=Lu, M=Cs

A paramagnetic center interacts with the surrounding nuclear spins by hyperfine coupling and changes the appearance of the NMR spectrum. In particular, owing to the large value of the electron magnetic moment, the dipolar interaction provides information over a much larger range than nuclear–nuclear dipolar couplings.[4]

[*] G. Kervern, Prof. L. Emsley, Dr. G. Pintacuda
Université de Lyon, CNRS/ENS Lyon/UCB-Lyon 1
Centre de RMN à Très Hauts Champs
5 rue de la Doua, 69100 Villeurbanne (France)
Fax: (+33) 4-7889-6761
E-mail: guido.pintacuda@ens-lyon.fr
Dr. A. D'Aléo, Dr. O. Maury
Université de Lyon, CNRS/ENS Lyon, Laboratoire de Chimie
46 Allée d'Italie, 69364 Lyon (France)
Dr. L. Toupet
CNRS/Université de Rennes
35042 Rennes (France)

[**] This work has been supported by the French ANR (JC05_44957, NT05_3_42676 and 08-BLAN-0035-01) and by EU (RII3-0264145). NMR spectra were recorded at the Rhone-Alpes Large Scale Facility for NMR.

Supporting information for this article is available on the WWW under http://dx.doi.org/10.1002/anie.200805302.

Molecular rotational motion in liquids, or magic-angle spinning in solids, averages most of this interaction. A nonzero effect in the NMR spectrum (the pseudo-contact shift, PCS) is left only when a metal possesses an anisotropic magnetic susceptibility tensor (χ).[5] The PCS depends on the position of a given nucleus with respect to the principal axes of the susceptibility tensor χ anchored on the metal center according to a well-defined geometrical dependence. This situation is readily visualized in Figure 1a, which plots the

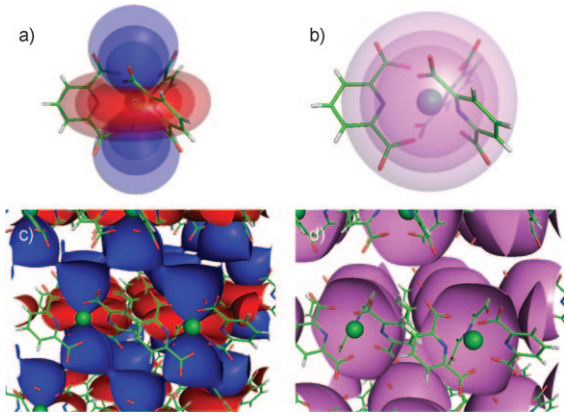

Figure 1. Isosurfaces for the pseudo-contact shift (a and c) and the axial anisotropy of the chemical shift tensor (b and d) superimposed on the structure of complex **1**, in the case of an isolated molecule (a and b) and in a crystalline lattice (c and d). Positive and negative PCS values are indicated by blue and red, respectively.

isosurfaces corresponding to different PCS values around the paramagnetic center in complex **1**. PCSs are easy to evaluate experimentally as long as through-bond (contact) interactions are negligible and provided an isostructural diamagnetic sample is available as a reference. PCSs are easy to model from the χ anisotropy and its orientation. PCSs are routinely used in solution NMR spectroscopy together with other data to refine structures,[6] to investigate protein–protein interactions,[7] or to monitor dynamics.[8]

The observation of PCSs in inorganic fragments[8] and notably for a microcrystalline paramagnetic protein[9] opens the perspective of their use in solid-state structure determination. Moreover, the tensor character of the paramagnetic shift is apparent in the solid state, resulting in increased information content.[10] The axial anisotropy $\Delta\sigma$ of the nuclear dipolar shift tensor is directly related to the electron–nucleus distance.[11] This effect is illustrated in Figure 1b, which presents surfaces of constant $\Delta\sigma$ around a metal center. This radial effect may thus offer a tool to disentangle the spatial

dependence of the PCSs to provide a measure of the molecular geometry, if the two effects could be measured at the same time.

Furthermore, in a microcrystalline sample, crystal packing exposes each nucleus to the field of all intermolecular paramagnets in addition to the one generated by the intramolecular metal center. Contributions from intercomplex hyperfine couplings are not negligible, particularly for small molecules. This situation results in shift tensors which notably deviate from axial symmetry, reducing the precision of intracomplex distances extracted from the shift anisotropies if the asymmetry η is not taken into account.[12]

However, to a good approximation, each of the surrounding paramagnetic centers contributes independently to the local fields on a given nucleus.[10] The total hyperfine dipolar Hamiltonian can thus be easily obtained by summing the dipolar interactions describing each electron–nucleus spin pair over the lattice (see the Supporting Information). Figure 1c,d shows how the network of metal centers in a crystal lattice alters the shape of the isosurfaces of PCS and $\Delta\sigma$. PCS and $\Delta\sigma$ interactions are thus probes of both the conformation of each molecule and simultaneously of the crystal packing.

The potential for structural investigations contained in these effects is demonstrated on molecules **1** and **2** in Figure 2. Each of these complexes was crystallized in two different space groups with different packing depending on the nature of the countercation (Figure 2a and b) while maintaining the same molecular geometry as determined by single-crystal X-ray diffraction (to within a root-mean-square deviation (RMSD) of 0.05 Å, see the Supporting Information). Figure 2 shows how the ^{1}H MAS NMR spectra of these compounds in powder form are dominated by the strong electron–nucleus interaction, with spinning sideband patterns extending over several hundred ppm owing to the anisotropy of the hyperfine interaction. The anisotropy changes considerably when crystal packing changes, thus providing a quantitative probe of both local and global geometry. Furthermore, the strength of the electron–nucleus interaction can be tuned by using lanthanides with increasing effective moments,[13] producing visible effects in the NMR spectrum in going, for example, from Yb^{III} ($\mu_{eff} = 4.5\,\mu_B$ Figure 2c,d) to Tb^{III} ($\mu_{eff} = 9.7\,\mu_B$ Figure 2e,f).

In the past, different nuclear spins (^{13}C,[11,12,15,16] ^{31}P,[17,18] ^{2}H,[19] ^{6}Li,[20] ^{7}Li[17,21]) have been employed to probe local structure. However, for all these nuclei, a fully quantitative evaluation of the paramagnetic effects was hampered by the large, non-negligible contribution from the diamagnetic chemical shift anisotropy (CSA) or contact interactions. In this regard, ^{1}H nuclei constitute a promising alternative, as they are 100% abundant, they have negligible CSA, they are rarely directly bonded to the metal center, and in solids they are not affected by Curie broadening, which is often a major obstacle to the NMR-spectroscopic study of paramagnetic molecules in solution.[22]

Traditionally, paramagnetic effects are more difficult to measure on ^{1}H because of the difficulty in signal assignment and the limited sensitivity and resolution in paramagnetic systems at natural abundance. Recently, we contributed to the development of a new approach for the efficient observation of 2D heteronuclear correlations on a paramagnetic sample at natural abundance.[12,23,24] In particular, spectra obtained through a combination of fast MAS, short adiabatic pulses,[14] and broadband heteronuclear (proton–carbon) recoupling sequences (e.g., transferred-echo double resonance, TEDOR)[16,24] can be acquired over a remarkably short experiment time, to record resolved proton and carbon signals with high sensitivity.

A ^{1}H,^{13}C TEDOR spectrum of compound **1a** is shown in Figure 3a. The spectrum shows two well-resolved patterns of correlations. The two sets of signals can be readily assigned to the *para* and *meta* protons of the aromatic ring on the basis of the integral of the ^{13}C direct excitation spectrum. Interest-

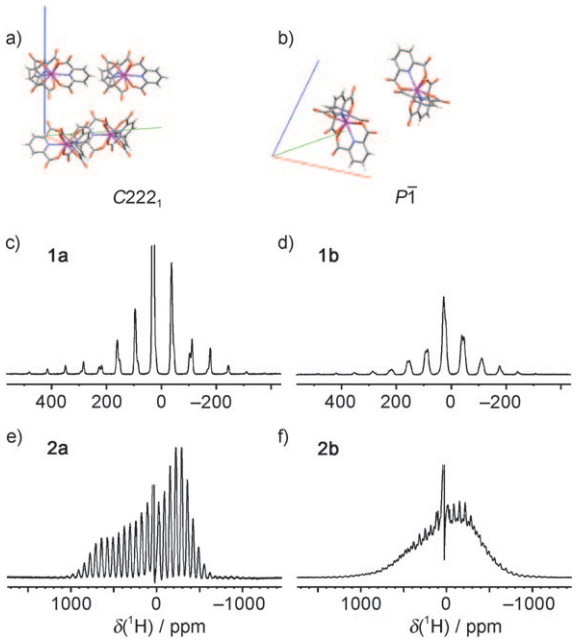

Figure 2. Representative crystal structures (a, b) and ^{1}H MAS spectra (33 kHz) of the complexes **1** (c, d) and **2** (e, f) crystallized with countercations Cs^+ (c, e) and Na^+ (d, f). All the spectra were acquired after a double adiabatic echo[14] without homonuclear decoupling.

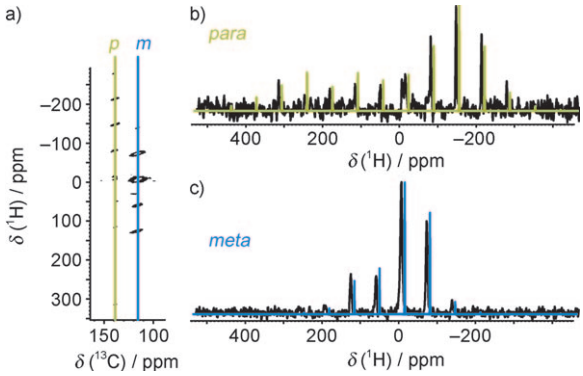

Figure 3. a) TEDOR spectrum of the complex **1a** (33 kHz). b, c) Traces extracted parallel to $\delta(^1H)$ corresponding to each proton-bearing carbon site. The yellow and blue lines represent the shift anisotropy patterns fitted according to reference [25].

ingly, the presence of two resonances indicates a local D_3 symmetry of the metal complex. Analysis of the sideband patterns in the ^{1}H dimension (Figure 3 b,c) according to reference [25] and neglecting ^{1}H–^{1}H and ^{1}H–^{13}C dipolar couplings yields the values of the isotropic and anisotropic shifts reported in Table 1. These values can be converted into paramagnetic PCSs and $\Delta\sigma$ after subtracting the corresponding diamagnetic contributions recorded for the isostructural diamagnetic Lu^{III} complex **3a** (Table 1).

Table 1: Experimental paramagnetic NMR spectroscopy parameters for complexes **1a** and **3a**, and corresponding values calculated for the structure determined by NMR spectroscopy with the lowest ε^2.

	meta ^{1}H		*para* ^{1}H	
	exp	calcd	exp	calcd
δ^{Yb}	4.3 ± 0.4		-4.3 ± 0.4	
δ^{Lu}	7.8 ± 0.1		6.7 ± 0.1	
PCS	-3.5 ± 0.5	-3.7 ± 0.4[a]	-11.0 ± 0.5	-10.3 ± 0.6[a]
$\Delta\sigma$	159.8 ± 4.4	174.2 ± 2[a]	426.1 ± 9.9	433 ± 40[a]
η	0.02 ± 0.12	0.23 ± 0.05[a]	0.2 ± 0.1	0.14 ± 0.07[a]

[a] Average value over all the (slightly inequivalent) proton sites.

With this data we can now determine the position of each nucleus with respect to the metal centers. Given the position of the metal centers and the orientation of their anisotropic χ tensors, the NMR spectrum of a given proton i can be back-calculated for any possible location (x,y,z) in the unit cell. We can then evaluate the difference with respect to the experimental isotropic and anisotropic paramagnetic shifts for each different proton [Eq. (1)]:[26]

$$\varepsilon^2[i](x,y,z) = \sum_x \frac{\left(X^{exp}[i] - X^{calcd}(x,y,z)\right)^2}{\Delta X^{exp}[i]^2} \qquad (1)$$

where $X^{exp}[i]$ and $X^{calcd}(x,y,z)$ are experimental and calculated values of the paramagnetic observable X ($X = \mathrm{PCS}, \Delta\sigma, \eta$) for proton i, and $\Delta X^{exp}[i]$ are the corresponding estimated errors.

Minimization of $\varepsilon^2[i]$ determines the position of each proton to be located on lines described by the intersection of the relevant isosurfaces of Figure 1 c, d. The location of these lines is broadened by the experimental errors $\Delta X^{exp}[i]$, which limit the precision of the determination of $\min(\varepsilon^2[i])$ to $\pm\Delta\varepsilon^2[i]$. Therefore, the isosurfaces corresponding to $\min(\varepsilon^2[i]) + \Delta\varepsilon^2[i]$ yield a confidence map for the location of each ^{1}H atom in the unit cell. Figure 4 a plots these surfaces for the whole crystal lattice, in a way reminiscent of the electron-density maps obtained in X-ray determinations. This result provides the basis for a structural determination that does not rely on the reciprocal position of two nuclei, but provides a tool to determine the absolute position of the ^{1}H atoms in a lattice.

Thus, confidence maps to determine ^{1}H positions can be generated given any metal position, the χ tensor anisotropy and orientation, and the crystal lattice parameters and symmetry. We envisage two main strategies for structure determination that can emerge.

In the first case, if the geometry of the heavy atoms is solved by X-ray diffraction, all these parameters except the $\Delta\chi$ anisotropy are available. Thus $\varepsilon^2[i]$ can be minimized by varying the CH bond lengths (and/or angles) together with $\Delta\chi$. In this way, $\Delta\chi$ can be determined, and at the same time the ^{1}H atom can be placed in the cell. In the present case, the data of Figure 3, combined with the heavy-atom positions of the known single-crystal structure determined by X-ray diffraction (see the Supporting Information), place the ^{1}H nuclei at a distance of 1.07 Å from the aromatic carbons (see Figure S2).

In the second case, and perhaps more importantly, we can show that the positions of the hydrogen sublattice can be identified even when the heavy-atoms positions are not known. In this case, if only the space group and lattice parameters are known (e.g., from powder X-ray diffraction[27]), the process can be used to obtain a full structural determination from NMR spectroscopy data, according to the following schematic protocol: 1) generate confidence maps which sample the paramagnetic degrees of freedom, that is, the metal position in the cell (x[M],y[M],z[M]), the orientation (α,β,γ) and anisotropy of its χ tensor ($\Delta\chi$); 2) generate a molecular model inside each of these maps, and screen the positional and orientational degrees of freedom of the ligands; 3) score the structures according to a global agree-

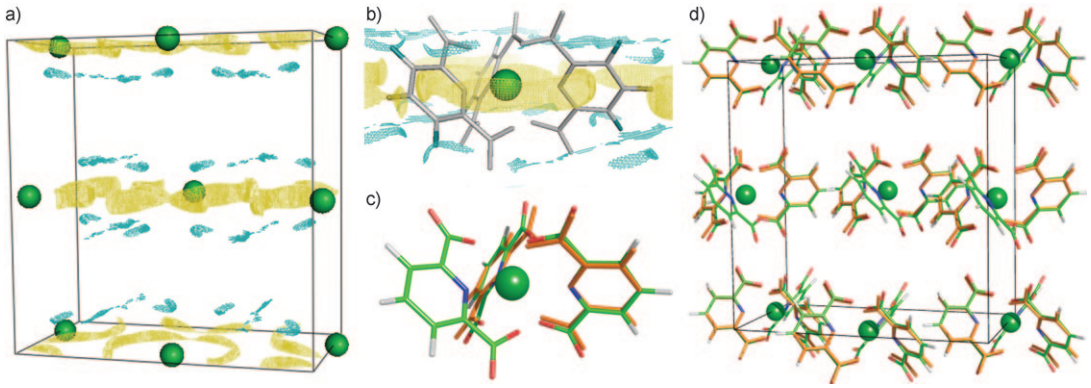

Figure 4. a) Agreement maps between experimental data and positions in the unit cell for the *meta* protons (blue mesh) and the *para* protons (yellow mesh) of complex **1a**. Meshes delimit regions with an agreement $\varepsilon^2[i] < \min(\varepsilon^2[i]) + \Delta\varepsilon^2[i]$ (with $\min(\varepsilon^2) = 12$; $\Delta\varepsilon^2 = 5$ for both types of protons). Metal positions and the χ tensor orientation are those obtained from the known crystal structure. b) Structure of complex **1a** obtained by fitting the rigid dipicolinate ligands into the agreement maps. c, d) Comparison of the experimentally determined structure (colored) from the known crystal structure (orange) for the isolated molecule (c) or a full asymmetric unit cell (d).

ment with the experimental data for the N protons of the complex [Eq. (2)]:

$$\varepsilon^2_{tot} = \frac{1}{N}\sum_{i}^{N} \varepsilon^2[i] \qquad (2)$$

and select the bundle of structures with an agreement lower than $\varepsilon^2_{tot} + \Delta\varepsilon^2_{tot}$ (i.e. all the structures that cannot be excluded by the experimental data given the errors $\Delta X^{exp}[i]$).

These three schematic steps are incorporated into a search algorithm that explicitly takes into account the periodicity of the solid-state problem, the symmetry evidenced by NMR spectroscopy, and the elements of structure that may be safely considered rigid in the ligand. Thus, notably the freedom of the metal ion in the cell is limited by the symmetry of the space group, allowing displacement only along the unique C_2 axis (i.e. parallel to the cell a axis). Local D_3 symmetry of the complex results in an axially symmetric χ tensor, oriented perpendicular to the C_2 axis. This arrangement limits the translational search in step 1 to the x[M] coordinate and the rotational search to the β angle. In the second step, the symmetry of the complex and the planarity and rigidity of this particular ligand reduce the conformational space of solutions. Modeling the ligand as a rigid unit limits the search to the r_{Ln-N} distance and rotation ϕ around the Ln–N axis. The rest of the complex is generated by applying two $2\pi/3$ rotations about the principal axis of the χ tensor, and the other cell mates are built by applying the group symmetry operations.

The final structures determined by applying this procedure to the data obtained in Table 1 from the spectrum of Figure 3 result in a structure with an ensemble RMSD of only 0.3 Å and with average coordinates that deviate from the structure determined by single-crystal X-ray diffraction by a RMSD of only 0.22 Å. Figure 4b–d shows the structure determined by this procedure.

In conclusion, the method described above provides unique information on the arrangement of paramagnetic molecules in the solid phase, determining molecular conformation as well as positions and orientations of neighboring molecules. The method exploits the particular potential of solid-state NMR spectroscopy to provide stronger structural restraints than in analogous solution-state approaches. The result is a full crystal structure determination of compound **1a** in powder form and at natural isotopic abundance that is found to be identical to that determined by single-crystal X-ray diffraction to within the error of the method. This work represents a further step forward in the fast-developing field of "NMR crystallography".[2,28]

Experimental Section

See the Supporting Information for full experimental procedures regarding sample preparation, a summary of crystallographic details, and solid-state NMR spectra acquisition and analysis.

Received: October 29, 2008
Revised: January 7, 2009
Published online: March 19, 2009

Keywords: lanthanides · NMR crystallography · NMR spectroscopy · paramagnetism · structure elucidation

[1] a) M. Baldus, *Angew. Chem.* **2006**, *118*, 1204–1207; *Angew. Chem. Int. Ed.* **2006**, *45*, 1186–1188; b) A. Böckmann, *Angew. Chem.* **2008**, *120*, 6200–6204; *Angew. Chem. Int. Ed.* **2008**, *47*, 6110–6113.
[2] B. Elena, G. Pintacuda, N. Mifsud, L. Emsley, *J. Am. Chem. Soc.* **2006**, *128*, 9555–9560; D. H. Brouwer, R. J. Darton, R. E. Morris, M. H. Levitt, *J. Am. Chem. Soc.* **2005**, *127*, 10365–10370; C. J. Pickard, E. Salager, G. Pintacuda, B. Elena, L. Emsley, *J. Am. Chem. Soc.* **2007**, *129*, 8932–8933; D. H. Brouwer, *J. Am. Chem. Soc.* **2008**, *130*, 6306–6307; R. K. Harris, *J. Pharm. Pharmacol.* **2007**, *59*, 225–239.
[3] N. Ouali, B. Bocquet, S. Rigault, P. Y. Morgantini, J. Weber, C. Piguet, *Inorg. Chem.* **2002**, *41*, 1436–1445.
[4] I. Bertini, C. Luchinat, G. Parigi, *Solution NMR of Parmagnetic Molecules: Application to Metallobiomolecules and Models*, Elsevier, Amsterdam, **2001**.
[5] I. Bertini, C. Luchinat, G. Parigi, *Prog. Nucl. Magn. Reson. Spectrosc.* **2002**, *40*, 249–273.
[6] I. Bertini, C. Luchinat, G. Parigi, *Concepts Magn. Reson.* **2002**, *14*, 259–286.
[7] G. Pintacuda, M. A. Keniry, T. Huber, A. Y. Park, N. E. Dixon, G. Otting, *J. Am. Chem. Soc.* **2004**, *126*, 2963–2970; G. Pintacuda, A. Y. Park, M. A. Keniry, N. E. Dixon, G. Otting, *J. Am. Chem. Soc.* **2006**, *128*, 3696–3702; G. Pintacuda, M. John, X. C. Su, G. Otting, *Acc. Chem. Res.* **2007**, *40*, 206–212.
[8] I. Bertini, C. Del Bianco, I. Gelis, N. Katsaros, C. Luchinat, G. Parigi, M. Peana, A. Provenzani, M. A. Zoroddu, *Proc. Natl. Acad. Sci. USA* **2004**, *101*, 6841–6846; X. Wang, S. Srisailam, A. A. Yee, A. Lemak, C. Arrowsmith, J. H. Prestegard, F. Tian, *J. Biomol. NMR* **2007**, *39*, 53–61.
[9] S. Balayssac, I. Bertini, K. Falber, M. Fragai, S. Jehle, M. Lelli, C. Luchinat, H. Oschkinat, K. J. Yeo, *ChemBioChem* **2007**, *8*, 486–489; S. Balayssac, I. Bertini, M. Lelli, C. Luchinat, M. Maletta, *J. Am. Chem. Soc.* **2007**, *129*, 2218–2219.
[10] A. Nayeem, J. P. Yesinowski, *J. Chem. Phys.* **1988**, *89*, 4600–4608.
[11] A. R. Brough, C. P. Grey, C. M. Dobson, *J. Am. Chem. Soc.* **1993**, *115*, 7318–7327.
[12] N. P. Wickramasinghe, M. A. Shaibat, C. R. Jones, L. B. Casabianca, A. C. de Dios, J. S. Harwood, Y. Ishii, *J. Chem. Phys.* **2008**, *128*, 052210.
[13] B. Bleaney, *J. Magn. Reson.* **1972**, *8*, 91–100.
[14] G. Kervern, G. Pintacuda, L. Emsley, *Chem. Phys. Lett.* **2007**, *435*, 157–162.
[15] S. Ganapathy, V. P. Chacko, R. G. Bryant, M. C. Etter, *J. Am. Chem. Soc.* **1986**, *108*, 3159–3165; K. Liu, D. Ryan, K. Nakanishi, A. McDermott, *J. Am. Chem. Soc.* **1995**, *117*, 6897–6906; T. M. de Swiet, J. L. Yarger, T. Wagberg, J. Hone, B. J. Gross, M. Tomaselli, J. J. Titman, A. Zettl, M. Mehring, *Phys. Rev. Lett.* **2000**, *84*, 717–720.
[16] P. Nalinda, N. P. Wickramasinghe, Y. Ishii, *J. Magn. Reson.* **2006**, *181*, 233–243.
[17] M. C. Tucker, M. M. Doeff, T. J. Richardson, R. Finones, J. A. Reimer, E. J. Cairns, *Electrochem. Solid-State Lett.* **2002**, *5*, A95–A98.
[18] W. L. Huang, M. Schopfer, C. Zhang, R. C. Howell, B. A. Gee, L. C. Francesconi, T. Polenova, *J. Phys. Chem. B* **2006**, *110*, 12340–12350; W. Huang, M. Schopfer, C. Zhang, R. C. Howell, L. Todaro, B. A. Gee, L. C. Francesconi, T. Polenova, *J. Am. Chem. Soc.* **2008**, *130*, 481–490.
[19] H. Lee, T. Polenova, R. H. Beer, A. McDermott, *J. Am. Chem. Soc.* **1999**, *121*, 6884–6894.

[20] A. K. Cheetham, C. M. Dobson, C. P. Grey, R. J. B. Jakeman, *Nature* **1987**, *328*, 706 – 707; Y. J. Lee, C. P. Grey, *J. Phys. Chem. B* **2002**, *106*, 3576 – 3582.
[21] C. P. Grey, Y. J. Lee, *Solid State Sci.* **2003**, *5*, 883 – 894; K. Kang, Y. S. Meng, J. Breger, C. P. Grey, G. Ceder, *Science* **2006**, *311*, 977 – 980.
[22] G. Kervern, S. Steuernagel, F. Engelke, G. Pintacuda, L. Emsley, *J. Am. Chem. Soc.* **2007**, *129*, 14118 – 14119.
[23] Y. Ishii, N. P. Wickramasinghe, S. Chimon, *J. Am. Chem. Soc.* **2003**, *125*, 3438 – 3439.
[24] G. Kervern, G. Pintacuda, Y. Zhang, E. Oldfield, C. Roukoss, E. Kuntz, E. Herdtweck, J. M. Basset, S. Cadars, A. Lesage, C. Coperet, L. Emsley, *J. Am. Chem. Soc.* **2006**, *128*, 13545 – 13552.
[25] P. Hodgkinson, L. Emsley, *J. Chem. Phys.* **1997**, *107*, 4808 – 4816.
[26] This value, often called χ^2, is here dubbed ε^2 to avoid confusion with the magnetic susceptibility.
[27] K. D. M. Harris, M. Tremayne, *Chem. Mater.* **1996**, *8*, 2554 – 2570.
[28] L. Beitone, C. Huguenard, A. Gansmuller, M. Henry, F. Taulelle, T. Loiseau, G. Ferey, *J. Am. Chem. Soc.* **2003**, *125*, 9102 – 9110; C. A. Fyfe, A. C. Diaz, H. Grondey, A. R. Lewis, H. Forster, *J. Am. Chem. Soc.* **2005**, *127*, 7543 – 7558.

